Multi-omics analyses identify molecular signatures with prognostic values in different heart failure aetiologies

Aboumsallem, Joseph Pierre; Shi, Canxia; De Wit, Sanne; Markousis-Mavrogenis, George; Bracun, Valentina; Eijgenraam, Tim R.; Hoes, Martijn F.; Meijers, Wouter C.; Screever, Elles M.; Schouten, Marloes E.

Published in:
Journal of molecular and cellular cardiology

DOI:
10.1016/j.yjmcc.2022.12.001

Publication date:
2023

Journal of Molecular and Cellular Cardiology 175 (2023) 13–28

Contents lists available at ScienceDirect

Journal of Molecular and Cellular Cardiology

journal homepage: www.elsevier.com/locate/yjmcc

Multi-omics analyses identify molecular signatures with prognostic values in different heart failure aetiologies

Joseph Pierre Aboumsallem [a,b], Canxia Shi [a], Sanne De Wit [a], George Markousis-Mavrogenis [a], Valentina Bracun [a], Tim R. Eijgenraam [a], Martijn F. Hoes [a], Wouter C. Meijers [a,b], Elles M. Screever [a,b], Marloes E. Schouten [a], Adriaan A. Voors [a], Herman H.W. Silljé [a], Rudolf A. De Boer [a,b,*]

[a] Department of Cardiology, University Medical Center Groningen, University of Groningen, Groningen, The Netherlands
[b] Department of Cardiology, Erasmus Medical Center, Rotterdam, The Netherlands

ARTICLE INFO

Keywords:
Multi-omics
Heart failure
Transcriptomics
Proteomics
Metabolomics
Cell death
Tissue repair
Autophagy
Polyamine
ATP

ABSTRACT

Background: Heart failure (HF) is the leading cause of morbidity and mortality worldwide, and there is an urgent need for more global studies and data mining approaches to uncover its underlying mechanisms. Multiple omics techniques provide a more holistic molecular perspective to study pathophysiological events involved in the development of HF.

Methods: In this study, we used a label-free whole myocardium multi-omics characterization from three commonly used mouse HF models: transverse aortic constriction (TAC), myocardial infarction (MI), and homozygous Phospholamban-R14del (PLN-R14$^{\Delta/\Delta}$). Genes, proteins, and metabolites were analysed for differential expression between each group and a corresponding control group. The core transcriptome and proteome datasets were used for enrichment analysis. For genes that were upregulated at both the RNA and protein levels in all models, clinical validation was performed by means of plasma level determination in patients with HF from the BIOSTAT-CHF cohort.

Results: Cell death and tissue repair-related pathways were upregulated in all preclinical models. Fatty acid oxidation, ATP metabolism, and Energy derivation processes were downregulated in all investigated HF aetiologies. Putrescine, a metabolite known for its role in cell survival and apoptosis, demonstrated a 4.9-fold ($p < 0.02$) increase in PLN-R14$^{\Delta/\Delta}$, 2.7-fold ($p < 0.005$) increase in TAC mice, and 2.2-fold ($p < 0.02$) increase in MI mice. Four Biomarkers were associated with all-cause mortality (PRELP: Hazard ratio (95% confidence interval) 1.79(1.35, 2.39), $p < 0.001$; CKAP4: 1.38(1.21, 1.57), $p < 0.001$; S100A11: 1.37(1.13, 1.65), $p = 0.001$; Annexin A1 (ANXA1): 1.16(1.04, 1.29) $p = 0.01$), and three biomarkers were associated with HF-Related Rehospitalization, (PRELP: 1.88(1.4, 2.53), $p < 0.001$; CSTB: 1.15(1.05, 1.27), $p = 0.003$; CKAP4: 1.18(1.02, 1.35), $P = 0.023$).

Conclusions: Cell death and tissue repair pathways were significantly upregulated, and ATP and energy derivation processes were significantly downregulated in all models. Common pathways and biomarkers with potential clinical and prognostic associations merit further investigation to develop optimal management and therapeutic strategies for all HF aetiologies.

1. Introduction

Heart failure (HF) is a clinical syndrome leading to considerable morbidity and mortality, as well as mounting healthcare costs. Despite advances in the understanding of its pathophysiology and treatment, the prevalence of HF is increasing due to a combination of the ageing of the population, the growing prevalence of comorbidities associated with incident HF, as well as general risk factors for HF [1,2]. As such, mechanistic studies are necessary to improve our understanding of the pathophysiology of HF, as well as to guide therapeutic interventions.

Many small animal models have been established for the investigation of pathological and molecular mechanisms contributing to HF in

* Corresponding author at: Department of Cardiology, Erasmus Medical Center, Rotterdam, The Netherlands
E-mail address: r.a.deboer@erasmusmc.nl (R.A. De Boer).

https://doi.org/10.1016/j.yjmcc.2022.12.001
Received 13 July 2022; Received in revised form 31 October 2022; Accepted 2 December 2022
Available online 6 December 2022

humans. Despite their limitations, these preclinical models have significantly enriched our knowledge of the pathogenesis of different aetiologies of HF and have the additional advantage of eliminating the potential confounding effects of genetic or environmental factors and comorbidities. The advent of omics analyses has allowed for detailed phenotyping of such models at the DNA, RNA, protein, metabolic and epigenetic levels. However, since omics approaches are relatively recent scientific developments, no standard working methods are universally employed, thus rendering the comparison of findings between studies with omics analyses difficult. In addition, many studies are limited to single-omics approaches, and not much is known regarding the concordance of omics findings at the RNA and protein levels.

The main goal of this study is to investigate heart tissues from three small animal models of HF [transverse aortic constriction (TAC), Myocardial Infarction (MI) [3,4], and a pathogenic variant in the Phospholamban gene (PLN-R14$^{\Delta/\Delta}$) [5]], using standardized label-free transcriptomics, proteomics and metabolomics analyses, so as to delineate their similarities and differences at the RNA, protein and metabolic levels, respectively.

Omics studies of human myocardial tissues are confounded by several factors, including disease state, tissue heterogeneity, comorbidities, and treatments, and are therefore difficult to standardize. Thus, using these clinically relevant animal models overcome these problems and provides libraries for investigators to pursue and assess any therapeutic target they see fit for their research interests (e.g. inhibiting a specific factor that is upregulated, or validating these factors in a different clinical database).

In this study, findings from small animal proteomics analyses were cross-referenced in the human setting, by checking their clinical relevance and prognostic value in patients with HF from the systems Biology Study to Tailored Treatment in Chronic Heart Failure (BIOSTAT-CHF) a large and diverse population of patients with HF that has been described previously in detail [6–9]. Moreover, the concordance of transcriptomic and proteomic analyses was investigated to address the necessity of performing both proteomic and transcriptomic analyses, in order to establish robust and complete scientific conclusions.

2. Materials and methods

2.1. Ethics

All experimental procedures in animals were approved by the animal ethical committee of the University of Groningen (permit numbers AVD105002016487, IVD16487–02-003, IVD16487–01-001, AVD10500201583 and IVD1583–02-001). The animal facilities at the University Medical Center Groningen are ISO-certified and follow national and EU regulations (Directive 2010/63/EU of the European Parliament on the protection of animals used for scientific purposes). All experiments involving animals were executed according to ARRIVE guidelines [10].

2.2. Experimental design and animal models

C57BL/6 J Charles River, France) male mice were randomized at the age of 8 weeks to receive either MI or no MI (Sham) surgery, as previously published [11]. Mice were intubated and mechanically ventilated with a 2% isoflurane/oxygen mixture using a rodent ventilator (Harvard Midivent). Body temperature was maintained at 37 °C. MI was inflicted by permanent ligation of the left anterior descending coronary artery using 6.0 prolene suture. MI- and sham-operated mice were followed-up for 6 weeks after surgery.

8-week-old male C57BL/6 J mice (Charles River, France) were randomized to either TAC surgery (using an o-ring with an inner diameter of 0.55 mm (part number: R00022–026-70BNB) from Apple Rubber (Lancaster, NY, USA)) or sham surgery.

Homozygous Phospholamban-R14del (PLN-R14$^{\Delta/\Delta}$) male mice and their controls (wild type) mice were generated as previously described [5]. Detailed surgical procedures are provided in supplementary methods. Animals were euthanized by dissecting the diaphragm under isoflurane anaesthesia, after which organs were harvested.

2.2.1. Echocardiography

Six weeks after TAC and MI surgery, and in 6 to 7-week-old PLN-R14$^{\Delta/\Delta}$ mice, transthoracic echocardiography was performed using a Vevo imaging station (FUJIFILM VisualSonics, Canada) and a Vevo 3100 preclinical imaging system (FUJIFILM VisualSonics), equipped with a 40-MHz MX550D linear array transducer (FUJIFILM VisualSonics). Prior to echocardiographic imaging, mice were anesthetized (2% isoflurane (TEVA Pharmachemie) mixed with oxygen, administered via an aerial dispenser) and the hair was removed from the thorax using a commercially available topical depilation agent with potassium thioglycolate (Veet). Mice were placed in supine position on the temperature-maintained (37 °C) platform of the Vevo imaging station (FUJIFILM VisualSonics) over the integrated electrode pads to monitor the heart and respiration rates. Short axis M-mode recordings of the left ventricles (LV) were obtained at the mid-papillary level. Vevo LAB software (version 5.5.0, FUJIFILM VisualSonics) was used to determine LV end-diastolic internal diameter, LV end-systolic internal diameter and fractional shortening by outlining the epicardial and endocardial borders using the LV Trace tool. For echocardiography measurements, the number of samples per group was as follows: TAC: $N = 9$, sham for TAC: $N = 5$; MI: $N = 6$, sham for MI: N = 6; PLN-R14$^{\Delta/\Delta}$: $N = 4$, WT: $N = 4$.

2.2.2. Sacrifice and collection of myocardial tissues

Animals were kept for 6 weeks after surgery (12 weeks of age for TAC and MI) and till the age of 6–7 weeks for the PLN-R14$^{\Delta/\Delta}$ mice. Mice were euthanized, and tissues, including the heart, were harvested and immediately snap frozen in liquid nitrogen and stored at −80 °C. Tissues were powdered prior to further processing.

2.3. Transcriptomics

2.3.1. RNA extraction and quality control

Total RNA was extracted from powdered left ventricle myocardium tissue samples using the SPLIT RNA Extraction Kit (Lexogen), according to the manufacturer's instructions. The number of samples per group was as follows TAC: $N = 6$, sham for TAC: $N = 4$; MI: $N = 5$, sham for MI: N = 4; PLN-R14$^{\Delta/\Delta}$: N = 4, WT: $N = 4$. Briefly, approximately 10 mg of tissue was homogenized in a highly chaotropic isolation buffer. After adding acidic buffer, acidic phenol and chloroform to the lysates, phases were separated using Phase Lock Gel tubes. RNA was precipitated onto a silica column by addition of isopropanol. Following washing steps, RNA was eluted from the column. Subsequently, RNA concentration was analysed by UV–Vis spectrophotometry (Nanodrop 2000c, Thermo Fisher), and RNA integrity was assessed on a Fragment Analyzer System using the DNF-471 RNA Kit (15 nt) (Agilent).

2.3.2. Library preparation, pooling and sequencing

Libraries were prepared manually according to the manufacturer's instructions using QuantSeq 3' mRNA-Seq FWD Library Prep Kit (Lexogen, UG Version 015UG009V0252). Briefly, 200 ng total RNA was denatured for 3 min at 85 °C with oligo(dT) primers containing an Illumina-compatible sequence at its 5′ end, followed by reverse transcription at 42 °C for 15 min. After RNA removal, the second strand of the cDNA was synthesized by a random primer containing an Illumina-compatible linker sequence at its 5′ end, and the end-product was purified by a magnetic bead-based method in order to remove all reaction components. Finally, individual sample barcodes (dual indexing) for multiplexing were introduced via 12 cycles of PCR (determined by qPCR); the left-over reaction components were removed by a magnetic bead-based purification method. All libraries were analysed for adapter

dimers, size distribution and concentration on a Fragment Analyzer System using the DNF-474 HS NGS Fragment kit (1–6000 bp) (Agilent). After pooling the libraries in an equimolar ratio, the concentration and the size distribution of the lane mix was analysed by Qubit dsDNA HS assay (Thermo Fisher Scientific) and by 2100 Bioanalyzer device using the HS-DNA assay (Agilent), respectively. A 2 nM dilution of the lane mix was denatured and diluted to loading concentration for sequencing on a NextSeq 500 instrument with SR75 High Output Kit (Illumina).

2.3.3. Sequencing quality control and adapter trimming

Using cutadapt version 1.18 (https://cutadapt.readthedocs.io/en/stable/), the reads of the sequencing run were scanned for adapter contaminations, continuous polyA sequences and continuous polyG sequences at the 3′ end, and the contaminations were removed if they were found. The reads of the samples prior to adapter trimming and after adapter trimming were analysed with FastQC version v0.11.7 (https://www.bioinformatics.babraham.ac.uk/projects/fastqc/).

2.3.4. Alignment and read quantification

The reads were aligned to the spike-in complemented Ensembl release 101 of the *Mus musculus* assembly GRCh38 from the Genome Reference Consortium. The alignment was performed with the splice-aware aligner STAR version 2.6.1a (https://github.com/alexdobin/STAR). The alignments were quantified based on the annotations of Ensembl GRCm38.101 and the spike-in specific annotations of Lexogen with the featureCounts software program version 1.6.4 of the subread analysis package (http://subread.sourceforge.net/).

2.3.5. Validation of omics data by quantitative PCR

The commonly upregulated genes in all three groups has been selected to be validated by RT qPCR (only genes with a log2FC higher equal or above to 1 has been selected for each group). Total RNA was isolated from left ventricular tissues (TAC and MI were induced as previously described [12]) using TRIzol reagent (Invitrogen Corporation, the Netherlands). RNA concentration of samples was measured by spectrophotometry (NanoDrop 2000, ThermoScientific, the Netherlands). cDNA was synthesized using QuantiTect Reverse Transcription kits (Qiagen). Gene expression levels were determined by qPCR analysis using iQ SYBR green supermix (Bio-Rad, CA, USA) and the Bio-Rad CFx384 real time system (Bio-Rad, the Netherlands)with 7.5 ng cDNA. For the gene expression validation by RT-qPCR, the number of samples per group was as follows:: TAC: $N = 8$, sham for TAC: $N = 10$; MI: $N = 9$, sham for MI: $N = 7$; PLN-R14$^{\Delta/\Delta}$: $N = 4$, WT: $N = 4$. Gene expressions were corrected for ribosomal protein, large, P0 (36B4) reference gene expression and are presented as relative expression to the control group. Primers used for RT-qPCR are presented in Supplementary table 2.

2.4. Proteomics

2.4.1. Tissue samples

Total protein was isolated from powdered left ventricle myocardium tissue samples by adding 10 µL ice-cold NP40 buffer (400 mM NaCl, 0.1% NP40 (Igepal-640), 10 mM TRIS pH 8.0 and 1 mM EDTA pH 8.0) per 1 mg of tissue. The samples were homogenized using the TissueLyzer LT (Qiagen, Hilden, Germany). Homogenized samples were centrifuged at 12,000*g* for 10 min at 4 °C. Next, the supernatant was collected, and protein concentrations were determined using a Pierce bicinchoninic acid (BCA) protein assay kit (Thermo Scientific, MA, USA) according to the manufacturer's protocol. For proteomics analysis, the number of samples per group was as follows: TAC: $N = 4$, sham for TAC: $N = 3$; MI: $N = 6$, sham for MI: N = 4; PLN-R14$^{\Delta/\Delta}$: N = 4, WT: $N = 4$.

Proteins samples (50 µg) were loaded on an 8% pre-cast RunBlue gel (Expedeon), and run at 100 V for 5 min. Gel staining was performed using InstantBlue (Expedeon) followed by a wash with ultrapure water. Coomassie-stained bands were excised in one gel slice that were further cut into small pieces and distained using 70% 50 mM NH_4HCO_3 and 30% acetonitrile. Reduction was performed using 10 mM DTT dissolved in 50 mM NH_4HCO3 for 30 min at 55 °C. Next, the samples were alkylated using 55 mM chloroacetamide in 50 mM NH_4HCO3 for 30 min at room temperature and protected from light. Subsequently, samples were washed for 10 min with 50 mM NH_4HCO_3 and for 15 min with 100% acetonitrile. Remaining fluid was removed and gel pieces were dried for 15 min at 55 °C. Tryptic digestion was performed by addition of sequencing-grade modified trypsin (Promega; 25 µL of 10 ng/mL in 50 mM NH_4HCO_3) and overnight incubation at 37 °C. Peptides were extracted using 5% formic acid in water followed by a second elution with 5% formic acid in 75% acetonitrile. Samples were dried in a SpeedVac centrifuge and dissolved in 20 µL 5% formic acid in water for analysis with LC-MS/MS.

2.4.2. Liquid chromatography

Online chromatography of peptides was performed with an Ultimate 3000 nano-HPLC system (Thermo Fisher Scientific) coupled online to an Orbitrap Exploris 480 mass spectrometer with a NanoFlex source (Thermo Fisher Scientific) equipped with a stainless-steel emitter. Tryptic digests were loaded onto a 5 mm 300 µm i.d. trapping micro column packed with PepMAP100 5 µm particles (Thermo Fisher Scientific) in 0.1% formic acid in water at the flow rate of 20 µL/min. After loading and washing for 3 min, peptides were forward-flush eluted onto a 50 cm 75 µm i.d. nanocolumn packed with Acclaim C18 PepMAP100 2 µm particles (Thermo Fisher Scientific). The following mobile phase gradient was delivered at the flow rate of 300 nL/min: 2–36% of solvent B in 112 min; 36–50% B in 10 min; 90% B during 4 min, and back to 2% B in 1 min and held at 2% B for 22 min. Total LC run is 152 min. Solvent A was 100:0 H_2O/acetonitrile (*v*/v) with 0.1% formic acid and solvent B was 0:100 H_2O/acetonitrile (v/v) with 0.1% formic acid.

2.4.3. Mass spectrometry

Mass spectrometry data were acquired using a data-dependent top-speed method dynamically choosing the most abundant not-yet-sequenced precursor ions from the survey scans (300–1650 Th @ 120,000 resolution) with a dynamic exclusion of 30 s and a cycle time of 3 s. Isolation of precursors was performed with a window of 1.6 Da. Resolution for HCD spectra was set to 15,000 at m/z 200. Normalized collision energy (NCE) was set at 28. Precursor ions with single, unassigned, or six and higher charge states were excluded from fragmentation selection. MS data were acquired for 130 min.

2.5. Metabolomics

2.5.1. Sample extraction

Each left ventricle myocardium tissue was weighted and transferred to an Eppendorf tube containing stainless steel beads and mixed with methanol/water (1:2). The Eppendorf tubes are placed in the bead beater and homogenized for 4 × 30 s. followed by ultra-sonication for 5 min. After centrifugation of the tubes the supernatant are collected, and the pellet are re-extracted by adding a new portion of methanol/water and repeating the process described above. Phospholipids are removed using Phree filters. The Filtrate from the Phree filters is collected and dried under a gentle nitrogen flow. Samples are reconstituted in six times initial sample weight using eluent mix. Filtrate the reconstituted samples using spinX filters, and collect the filtrate for analysis. For metabolomics analysis, the number of samples per group was as follows: TAC: $N = 6$, sham for TAC: $N = 4$; MI: N = 6, sham for MI: N = 4; PLN-R14$^{\Delta/\Delta}$: N = 4, WT: $N = 4$.

2.5.2. Semi-polar metabolites (LC-MS method)

The analysis was carried out using a UPLC system (Vanquish, Thermo Fisher Scientific) coupled with a high-resolution quadrupole-orbitrap mass spectrometer (Q Exactive™ HF Hybrid Quadrupole-Orbitrap, Thermo Fisher Scientific). An electrospray ionization interface was

used as ionization source. Analysis was performed in negative and positive ionization mode. A QC sample was analysed in MS/MS mode for identification of compounds. The UPLC was performed using a slightly modified version of the protocol described by Catalin et al. (UPLC/MS Monitoring of Water-Soluble Vitamin Bs in Cell Culture Media in Minutes, Water Application note 2011, 720004042en).

2.5.3. Data processing

Data was processed using Compound Discoverer 3.1 (ThermoFisher Scientific) and TraceFinder 4.1 (ThermoFisher Scientific). Compound extraction and Identification methods are detailed in supplementary methods.

2.6. Validation in clinical data

To validate the findings of the animal studies in humans, we used data from the BIOSTAT-CHF cohort, a large and diverse population of patients with HF that has been described previously [6–9]. Briefly, BIOSTAT-CHF was a multi-center study with 11 participating European countries. Participants were aged 18 years or older, had symptoms of new-onset or worsening HF, combined with a left ventricular ejection fraction (LVEF) ≤40% or brain-type natriuretic peptide (BNP) and/or N-terminal pro-BNP (NT-proBNP) plasma levels >400 pg/mL or > 2000 pg/mL, respectively. Participants were either not previously treated with angiotensin converting enzyme inhibitors/angiotensin receptor blockers and/or β-adrenoreceptor blockers or were receiving ≤50% of guideline-recommended target doses and anticipated their initiation or up-titration. All patients were treated with loop diuretics. Participants could be enrolled as inpatients or outpatients. The primary outcome was a composite of all-cause mortality and rehospitalization for HF censored at 2-year follow-up, and each outcome was also examined separately as a secondary outcome. The study protocol was approved by local and national ethics committees (EudraCT 2010–020808-29; R&D Ref Number 2008-CA03; MREC Number 10/S1402/39) and all participants provided written informed consent.

Here, we used plasma biomarker measurements (Olink Proteomics) of 362 biomarkers as described previously [6–9]· and contrasted those to genes that were significantly upregulated at the transcriptomic and proteomic levels in any of the examined models. Subsequently, we isolated only genes that were significant at both the transcriptomic and proteomic levels in any animal model for subsequent analyses. Selected biomarkers were evaluated for their relationship with clinical characteristics and outcomes (all-cause mortality and HF-related rehospitalization at 2-year follow-up).

2.7. Statistical analysis

For animal studies,. Variables were compared using the *t*-test. A *p*-value <0.05 was considered significant. Statistical analyses performed using GraphPad Prism 8.4.2 (GraphPad, San Diego, CA, USA). Gene expression analysis was conducted using DESeq2 (version v1.18.1). The analysis used the counts of unique alignments.

For proteomic data, raw mass spectrometry data were analysed using MaxQuant version, 1.6.3.4 using default settings and LFQ/iBAQ enabled [2]· and searched against the Uniprot/Swissprot database (was downloaded from Uniprot on 4/22/2021 and had 17,509 reviewed entries). The data was further processed using Perseus software, version 1.6.15.0.

For metabolomics, data are presented, in heatmaps, as the log2 values of the ratio between average values and *p*-values. Biological processes enrichment analyses were performed using the gene and protein sets [13]. A false discovery rate (FDR) < 0.05 is considered significant. Visualisations for all Omics analyses were generated using R-Studio (v.4.1.2). Principal Component Analysis (PCA) was used to visualize sample-to-sample variance. The input for this analysis were normalized read counts obtained with the rlog transformation of DESEq2.

Clinical data were analysed using R-Studio (v.4.1.2)., Normally distributed variables are presented as mean (standard deviation), non-normally distributed continuous variables as median (interquartile range), and categorical variables as number (percentage). The correlation of available biomarkers with clinical characteristics were examined with Spearman's rank order correlation and graphically displayed in the form of a heatmap. *P*-values of correlation analyses were adjusted for multiple comparisons using the Benjamini-Hochberg method. The association of the same biomarkers with outcomes censored at 2-year follow-up were examined for a combined outcome of all-cause mortality and HF-related rehospitalization and for all-cause mortality alone using Cox regression, and with competing-risks regression for HF-related rehospitalization alone. Analyses were carried out both for each biomarker individually, and with multivariable corrections for previously published risk models for each of the three outcomes [9].

2.8. Gene ontology analyses

The ShinyGO enrichment tool (version 0.76) (http://bioinformatics.sdstate.edu/go/ (accessed on 21 April 2021) [13]) was used for exploring enrichment in Gene Ontology (GO) categories for biological processes using the lists of up and down regulated genes and proteins ($p < 0.05$). Biological processes with false discovery rate (FDR) < 0.05 were considered significant. The web-server STRING (https://www.ncbi.nlm.nih.gov/pmc/articles/PMC6323986/)was employed to perform interaction analysis and to validate the pathways of interest. Biological processes with false discovery rate (FDR) < 0.05 were considered significant.

2.9. Annotations

For transcriptomic data, the alignments were quantified based on the annotations of Ensembl GRCm38.101 and the spike-in specific annotations of Lexogen with the featureCounts software program version 1.6.4 of the subread analysis package (http://subread.sourceforge.net/). Each gene has an ENSG ID and a gene name. As for proteins, the data was processed using Perseus software, version 1.6.15.0 and each protein has a ENSG ID and a gene name. Data was harmonized and the overlap between transcriptomic and proteomic was determined using the ENSG IDs and gene names. For metabolomics, the lists of detected compounds were submitted to metaboanalyst (https://www.metaboanalyst.ca/MetaboAnalyst/Secure/process/NameMapView.xhtml). Only compounds with Query names with the exact match were selected for further analyses.'

3. Results

3.1. TAC, MI, and PLN-R14$^{\Delta/\Delta}$ mice developed HF with reduced ejection fraction

Six weeks post-TAC surgery, the average left ventricular ejection fraction (LVEF) was 2-fold ($p < 0.0001$) lower than in sham-operated mice (Fig. 1A). Normalized heart weights were two times larger than the sham group, which indicates that TAC hearts were hypertrophic (Table 1). A 2.9-fold ($p = 0.0001$) higher lung weight was detected in TAC mice compared to their sham group (Table 1), attributed to pulmonary congestion and edema. (See Table 1.)

MI mice also demonstrated a reduced LVEF (1.6-fold lower, $p < 0.01$) (Fig. 1A) with dilation of the left ventricle inner diameter by 1.3-fold ($p < 0.01$) and 1.5-fold ($p < 0.01$) at diastole and systole, respectively (Fig. 1B and C). Normalized organ weights of the MI and sham-MI groups are presented in Table 2.

The PLN-R14$^{\Delta/\Delta}$ mouse model develops HF in an accelerated manner. At the age of six weeks, PLN-R14$^{\Delta/\Delta}$ had heavier wet lung weights (1.2-fold bigger than the WT mice, $p < 0.01$), suggesting pulmonary congestion and edema (Table 3). As shown previously [14]·

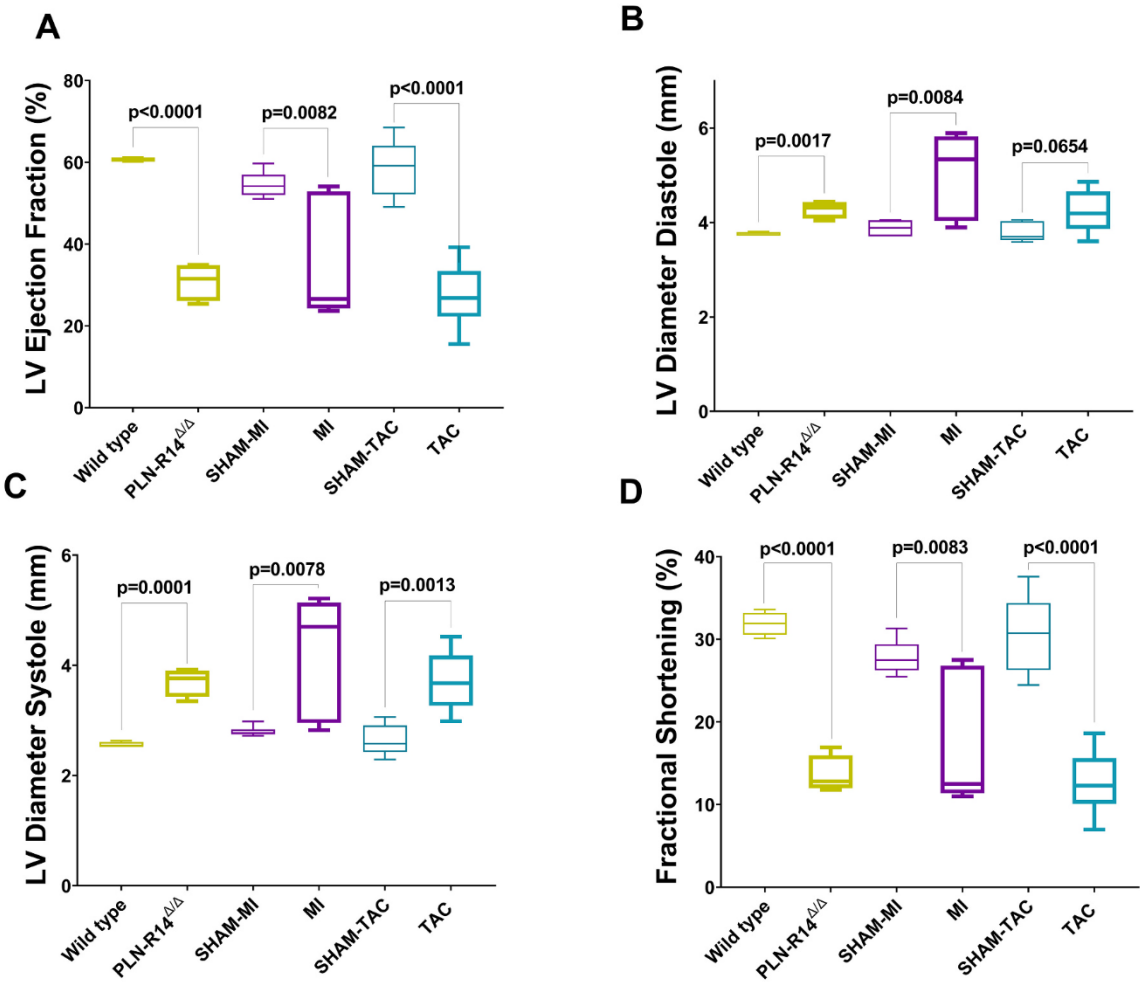

Fig. 1. Echocardiography measurements per model compared with their corresponding controls (sham-operated animals or wild type). Left ventricular (LV) ejection fraction (A). LV inner diameter diastole (B). LV inner diameter systole (C). LV fractional shortening (D). (TAC: $N = 9$, sham for TAC: $N = 5$; MI: $N = 6$, sham for MI: N = 6; PLN-R14$^{\Delta/\Delta}$: $N = 4$, WT: N = 4). Echo data for the PLN-R14$^{\Delta/\Delta}$ vs. wild type mice were previously published [14]. Data are presented as mean ± SEM. Variables were compared using the *t*-test. A *p*-value <0.05 was considered significant.

Table 1
Organ weight (normalized for tibia length (mg/mm)) in TAC vs. Sham for TAC.

	Sham-TAC (n = 5)	TAC (n = 9)	p-value (TAC vs. sham)
Heart	8.46 (0.3)	16.96 (0.8)	<0.0001
Left atria	0.15 (0.014)	0.53 (0.086)	0.0073
Right atria	0.12 (0.014)	0.26 (0.036)	0.0133
Lungs	9.09 (0.6)	26.02 (2.19)	0.0001
Liver	88.26 (2.178)	82.03 (3.56)	0.2462
Kidneys	20.03 (2.2)	20.66 (0.41)	0.7164
Spleen	3.77 (0.08)	4.87 (0.15)	0.0002

Table 2
Organ weight (normalized for tibia length (mg/mm)) in MI vs. Sham for MI.

	Sham-MI (n = 6)	MI (n = 6)	p-value (MI vs. Sham)
Heart	8.42 (0.23)	11.24 (0.42)	0.0002
Left atria	0.16 (0.0065)	0.22 (0.021)	0.0346
Right atria	0.2 (0.018)	0.16 (0.01)	0.0909
Lungs	8.26 (0.7)	8.43 (0.27)	0.8220
Liver	88.9 (2.78)	80.45 (3.29)	0.0777
Kidneys	21.99 (0.54)	23.55 (062)	0.0859
Spleen	4.15 (0.14)	4.41 (0.39)	0.3599

Table 3
Organ weight (normalized for tibia length (mg/mm)) in the PLN-R14$^{\Delta/\Delta}$ vs. wild type.

	WT (n = 4)	PLN-R14$^{\Delta/\Delta}$ (n = 4)	p-value (PLN-R14$^{\Delta/\Delta}$ vs. WT)
Heart	7.3 (0.45)	8.0 (0.42)	0.2942
Left atria	0.1 (0.013)	0.15 (0.017)	0.0627
Right atria	0.16 (0.037)	0.28 (0.088)	0.2458
Lungs	8.28 (0.3)	10.05 (0.36)	0.0091
Liver	73.9 (5.47)	70.12 (4.48)	0.6121
Kidneys	17.36 (1.17)	18.19 (0.91	0.5952
Spleen	4.72 (0.52)	5.88 (0.47)	0.1461

PLN-R14$^{\Delta/\Delta}$ LVEF was 2-fold lower ($p < 0.0001$) than the wild-type mice (Fig. 1A), and the left ventricular inner diameters were 1.1-fold ($p < 0.05$) and 1.4-fold (p = 0.0001) larger at the diastole and systole, respectively (Fig. 1B and C).

3.2. Transcriptomics and proteomic analyses

3.2.1. TAC, MI, and PLN-R14$^{\Delta/\Delta}$ mice represented distinct and common molecular signatures

The largest number of differentially expressed genes (DEG) and proteins (DEP), compared with the corresponding control group, were

observed in PLN-R14$^{\Delta/\Delta}$ mice (Fig. 2).This indicates that the genetic manipulation in the PLN-R14$^{\Delta/\Delta}$ model had a greater impact on gene and protein expressions than surgically induced HF models, TAC and MI. Myosin Heavy Chain 7 was detected as the most upregulated gene in MI (log2FC = 1.71, $p_{adj} < 0.0005$) and TAC (log2FC = 3.44, $p_{adj} < 0.0001$) (Fig. 2B, C). As for PLN-R14$^{\Delta/\Delta}$, TIMP Metallopeptidase Inhibitor 1 was the most upregulated gene (log2FC = 2.83, $p_{adj} < 0.0001$) (Fig. 2 A). The complete lists of differentially expressed genes are provided in Supplementary file. The top altered genes in all three models (with an absolute value of log2FC ≥ 1 were validated by quantitative PCR (Fig. 3). The list of these genes is also provided in supplementary table 2.

3.2.2. TAC exhibited a strong discordance between gene and protein expression trends

To compare the expression trends at the transcriptomic and proteomic levels, scatter plots were made to display the differential expression of genes (log2FC) versus their corresponding protein expression (difference between the means of the animal model and its corresponding control) (Fig. 4). More than half of the DEG-DEP pairs had discordant expression trends in TAC mice (53%) (Fig. 4A). Further, the MI model demonstrated a 35% discordance between DEGs and DEPs (Fig. 4B). As for PLN-R14$^{\Delta/\Delta}$ mice, the majority of pairs showed similar expression trends (25.7% discordant pairs) (Fig. 4C). Galectin 3 showed a strong concordance in expression trends at the transcriptomic (log2FC = 3.27, $p_{adj} < 0.0001$) and proteomic levels in PLN-R14$^{\Delta/\Delta}$ and MI models. However, TAC mice demonstrated a prounounced over-expression of the Galectin 3 gene (log2FC = 2.18, $p_{adj} < 0.0001$) but not the protein (Fig. 4A, B, C). The complete lists of differentially expressed proteins are provided in Supplementary file.

3.2.3. Cell death and tissue-repair pathways were upregulated in all HF mouse models

For this analysis, we checked for the overlapping processes that were enriched (using the complete list of DEGs and DEPs) in each model at the proteomic and transcriptomic levels. Common up- and downregulated processes in all three models are presented in Fig. 5. Thirteen processes were upregulated in TAC, MI, and PLN-R14$^{\Delta/\Delta}$ models. *Regulation of transport,* a process that modulates the movement of substances such as ions) by means of transporters or pores, was upregulated all the animal models (PLN-R14$^{\Delta/\Delta}$: FDR = 4.7×10^{-10}; MI: FDR = 6.2×10^{-10}; TAC: FDR = 0.02) (Fig. 5A). *Programmed cell death* (PLN-R14$^{\Delta/\Delta}$: FDR = 2.8×10^{-8}; MI: FDR = 2.7×10^{-5}; TAC: FDR = 0.02)and *apoptotic process* (PLN-R14$^{\Delta/\Delta}$: FDR = 1×10^{-7}; MI: FDR = 3.9×10^{-5}; TAC: FDR = 0.02) were enriched as upregulated processes in all three models (Fig. 5A). Moreover, the commonly enriched *response to wounding* process (PLN-R14$^{\Delta/\Delta}$: FDR = 4.1×10^{-5}; MI: FDR = 0.00028; TAC: FDR = 0.0048) indicates a change in the state or activity of cardiac cells, such as movement and secretion as a consequence of a stimulus caused by a damage. On the other hands, the process *wound healing* (PLN-R14$^{\Delta/\Delta}$: FDR = 8.3×10^{-5}; MI: FDR = 0.00017; TAC: FDR = 0.006) is a sequence of events that restores tissue integrity, following an injury (Fig. 5A). The processes *Response to oxygen-containing compound* (PLN-R14$^{\Delta/\Delta}$: FDR = 5.07×10^{-9}; MI: FDR = 5.87×10^{-7}; TAC: FDR = 0.047) and *Response to inorganic substance* (PLN-R14$^{\Delta/\Delta}$: FDR = 3.74×10^{-11}; MI: FDR = 5.79×10^{-12}; TAC: FDR = 0.0055) suggest that cardiac cells change their state and activity due to inorganic substance or oxygen-containing compound response to oxygen-containing compound (Fig. 5A). The complete lists of upregulated processes (in each model) are provided in Supplementary file.

3.2.4. Energy derivation processes were downregulated in all HF mouse models

Enrichment analyses demonstrated a shift towards the use of less energy-efficient free fatty acids. This shift was presented by the downregulation of *fatty acid oxidation* (PLN-R14$^{\Delta/\Delta}$: FDR = 4.14×10^{-26}; MI: FDR = 0.001; TAC: FDR = 1.1×10^{-6}), fatty acid beta-oxidation (PLN-R14$^{\Delta/\Delta}$: FDR = 4.14×10^{-26}; MI: FDR = 0.00145; TAC: FDR = 1.42×10^{-6}), and *lipid oxidation* (PLN-R14$^{\Delta/\Delta}$: FDR = 1×10^{-26}; MI: FDR = 0.0012; TAC: FDR = 1.52×10^{-6}) in all three HF mouse models (Fig. 6A). Moreover, this analysis showed that the *ATP metabolic process* (PLN-R14$^{\Delta/\Delta}$: FDR = 2.09×10^{-51}; MI: FDR = 3×10^{-13}; TAC: FDR = 0.0028), and *Energy derivation by oxidation of organic compounds* were downregulated in myocardial tissues of the three mouse models of HF (PLN-R14$^{\Delta/\Delta}$: FDR = 2.28×10^{-25}; MI: FDR = 1.09×10^{-17}; TAC: FDR = 0.00015), (Fig. 6A). Furthermore, the *ribonucleotide biosynthetic process* was significantly downregulated in these models (Fig. 6B). The complete lists of downregulated processes (in each model) are provided in Supplementary file.

3.3. Clinical relevance of the upregulated genes and proteins

3.3.1. Several upregulated genes were associated with NT-proBNP levels

Out of the 368 Olink plasma biomarkers previously measured in BIOSTAT-CHF [6–9]' seven genes were significantly upregulated at both the transcriptomic and proteomic levels in HF mouse models (Fig. 7A). The correlation of these seven biomarkers with clinical characteristics was examined with Spearman's rank order correlation and graphically displayed in the form of a heatmap (Fig. 7B). The patients included in this analysis have high levels of NT-proBNP 2028 [800.00, 4789.00] pg/mL (Supplementary Table 1). The majority (65%) of these patients have heart failure with reduced ejection fraction (LVEF<40%) (Supplementary Table 1). Proline And Arginine Rich End Leucine Rich Repeat Protein (PRELP) and Cytoskeleton Associated Protein 4 (CKAP4) showed the strongest positive correlation with NT − proBNP levels in HF patients ($p < 0.001$) (Fig. 7B).

3.3.2. Upregulated genes and proteins in animal models predicted HF-related rehospitalization, and all-cause mortality in HF patients

The association of the same biomarkers with outcomes censored at 2-year follow-up was assessed in the index cohort [7]. After multivariable corrections, four biomarkers were correlated to all-cause mortality (PRELP: 1.79(1.35, 2.39), $p < 0.001$; CKAP4: 1.38(1.21, 1.57), $p < 0.001$; S100 Calcium Binding Protein A11 (S100A11): 1.37(1.13, 1.65), $p = 0.001$; Annexin A1 (ANXA1): 1.16(1.04, 1.29) $p = 0.01$) (Table 4). Moreover, three biomarkers were associated with HF-Related Rehospitalization, after multivariable adjustments (BIOSTAT-CHF risk model) (PRELP: 1.88(1.4, 2.53), $p < 0.001$; CSTB: 1.15(1.05, 1.27), $p = 0.003$; CKAP4: 1.18(1.02, 1.35), $P = 0.023$) (Table 4).

3.4. Metabolomic analyses

3.4.1. Polyamines expression confirmed the upregulated cell death pathways at the protein level

Metabolomic analyses of cardiac tissues identified differentially expressed metabolites between each model and its control. A few metabolites were commonly altered in all three HF models TAC, MI, and PLN-R14$^{\Delta/\Delta}$. The natural diamine putrescine and polyamine spermine are low-molecular-weight organic polycations. They are well established for their role in cardiac physiology as key mediators of cell growth, proliferation, and division [15]. Putrescine showed a 4.9-fold ($p < 0.02$) increase in PLN-R14$^{\Delta/\Delta}$, 2.7-fold ($p < 0.005$) increase in TAC mice, and 2.2-fold ($p < 0.02$) increase in MI mice (Fig. 8H). As for spermine, it was only significantly upregulated in PLN-R14$^{\Delta/\Delta}$ mice (4.8-fold, $p < 0.005$) (Fig. 8I).

3.4.2. Altered metabolic and energy pathways were validated at the metabolomic level

Cardiac carnitine is vital for mammalian hearts to meet the energy requirements through the oxidation of long-chain fatty acids and regulation of carbohydrate metabolism [16,17]. Myocardial carnitine levels were decreased in all three models by approximately 1.1-fold in MI ($p < 0.05$), 1.2-fold in TAC ($p < 0.005$), and 11.4-fold in PLN-R14$^{\Delta/\Delta}$ ($p <$

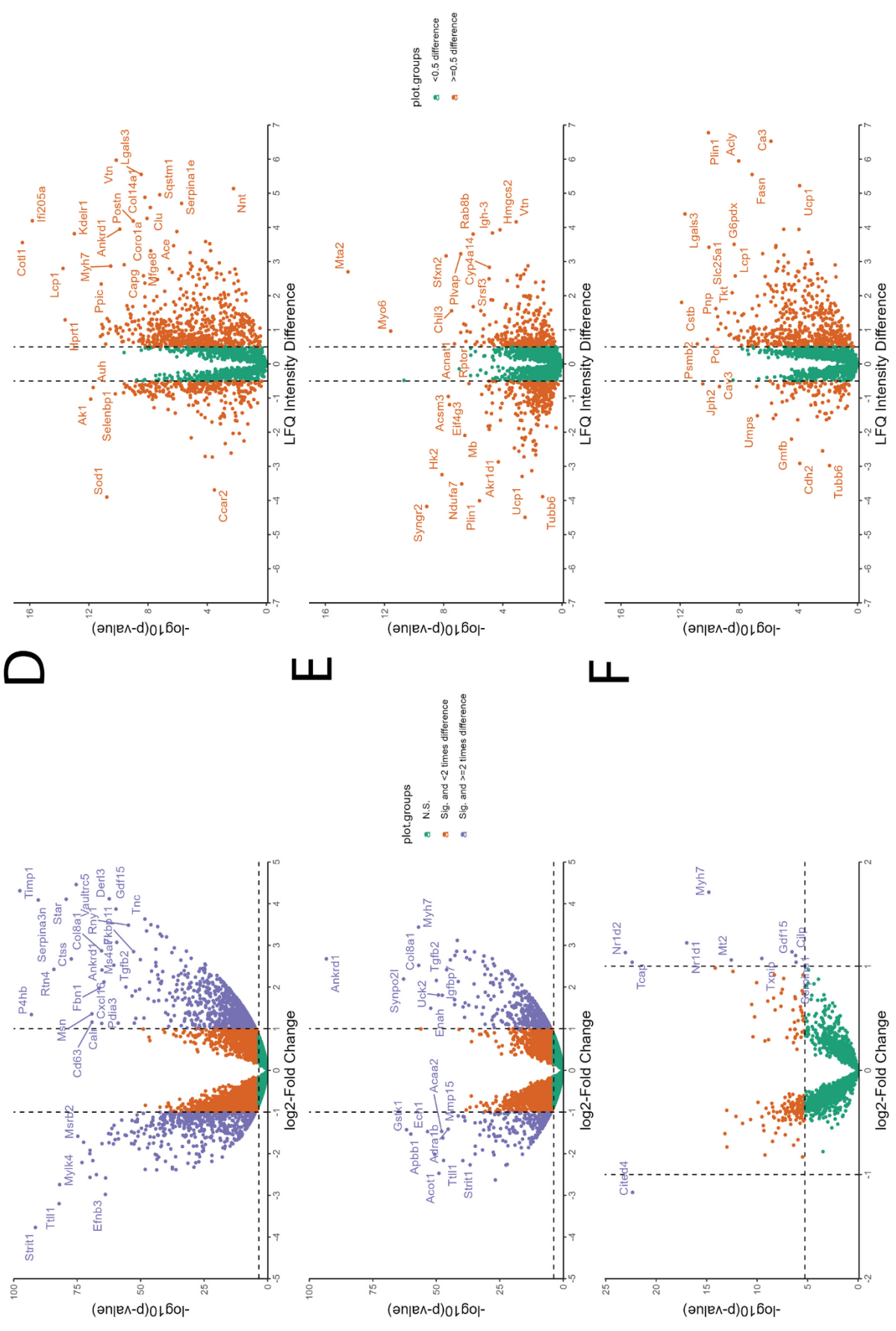

Fig. 2. Differential gene expression analysis. Volcano plots showing differentially expressed genes significance corresponds to -log(*p*-value). PLN-R14$^{\Delta/\Delta}$ vs. wild type mice (A). TAC vs. sham for TAC (B); MI vs. sham for MI (C); . (TAC: $N = 6$, sham for TAC: $N = 4$; MI: $N = 5$, sham for MI: N = 4; PLN-R14$^{\Delta/\Delta}$: N = 4, WT: N = 4). Differential protein expression analysis. Volcano plots showing differentially expressed proteins, significance corresponds to -log(p-value). Difference corresponds to the difference between LFQ averages of two groups. PLN-R14$^{\Delta/\Delta}$ vs. wild type mice (D). TAC vs. sham for TAC (E); MI vs. sham for MI (F); (TAC: N = 4, sham for TAC: $N = 3$; MI: N = 6, sham for MI: N = 4; PLN-R14$^{\Delta/\Delta}$: N = 4, WT: N = 4).

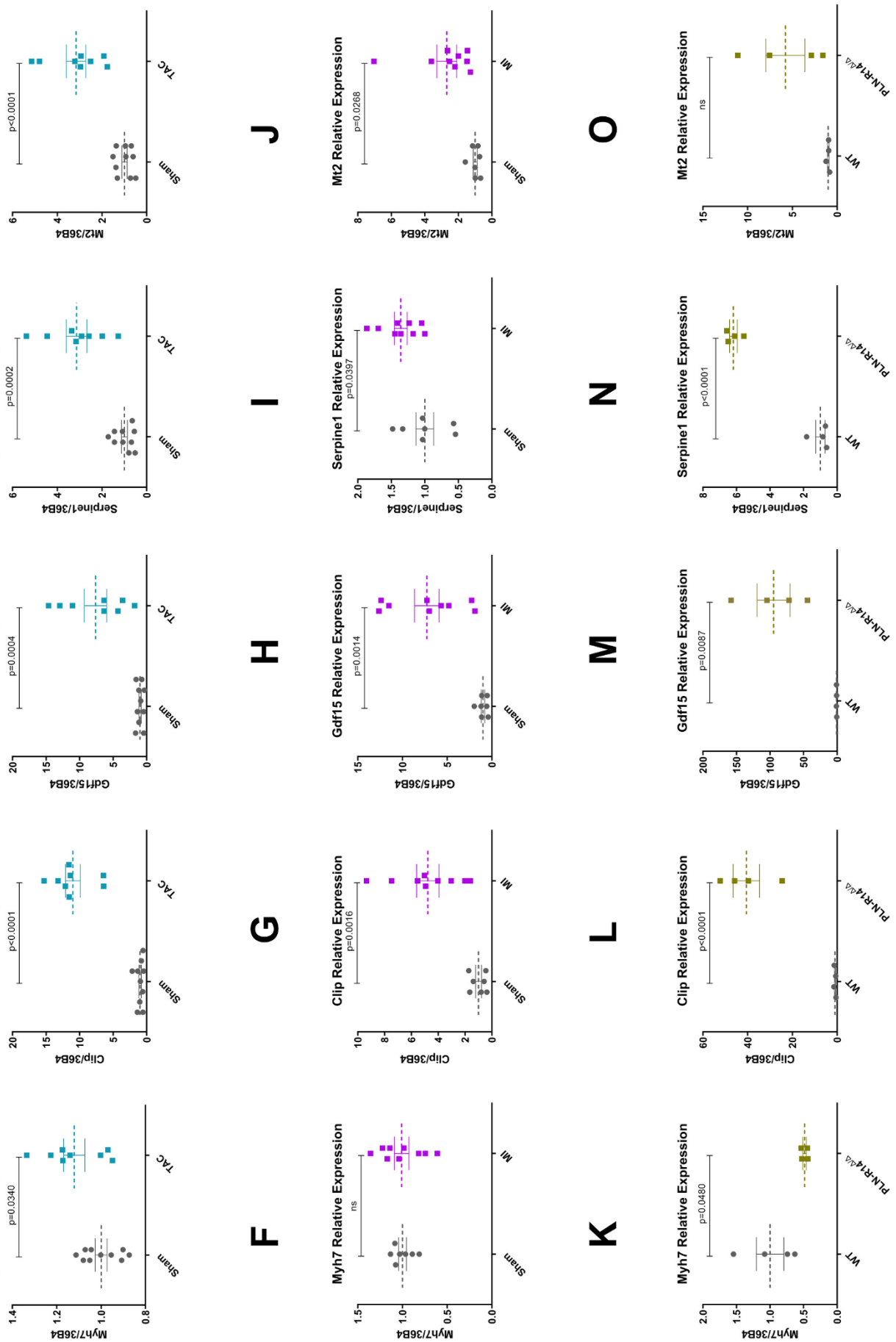

Fig. 3. Individual value plots of the qPCR measurements of mRNA levels of the common differentially expressed genes: Myh7, Cilp, Gdf15, Serpine1, Mt2 in TAC vs. sham for TAC (TAC: $N = 8$, sham for TAC: $N = 10$) (A-E); MI vs. sham for MI (MI: $N = 9$, sham for MI: $N = 7$) (F-J); PLN-R14$^{\Delta/\Delta}$ vs. WT mice (PLN-R14Δ/Δ: N = 4, WT: N = 4) (K-O). Data are presented as mean ± SEM. Variables were compared using the *t*-test. A p-value <0.05 was considered significant.

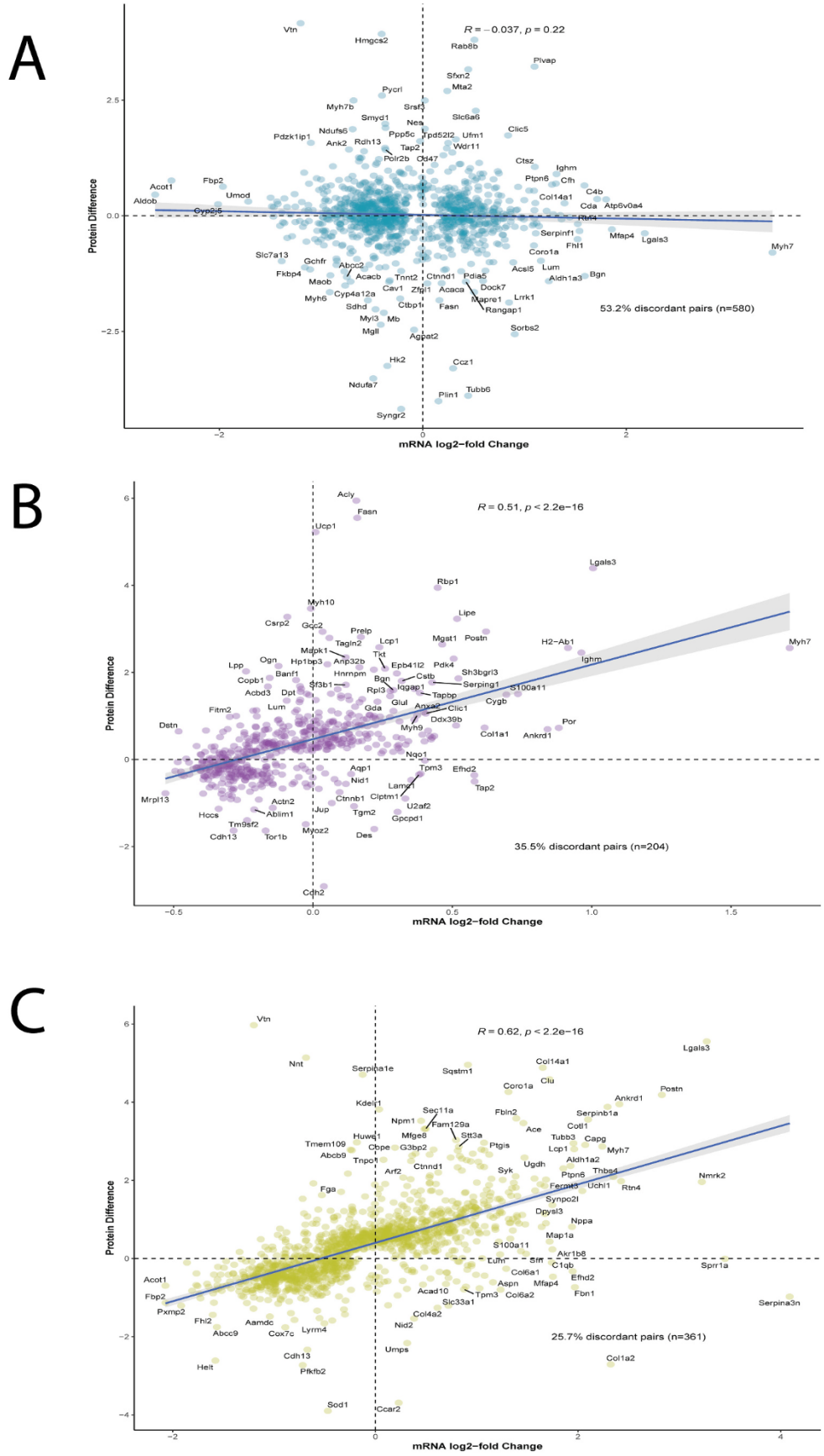

Fig. 4. Scattor plots displaying the levels of gene expression (log2FC between a specific model vs. its corresponding control) vs. protein expression (the term 'protein difference' corresponds to the difference between LFQ averages of a models and its corresponding control) for TAC (A), MI (B) and PLN-R14$^{\Delta/\Delta}$ (C). Only genes or proteins with a p-value <0.05 are plotted.

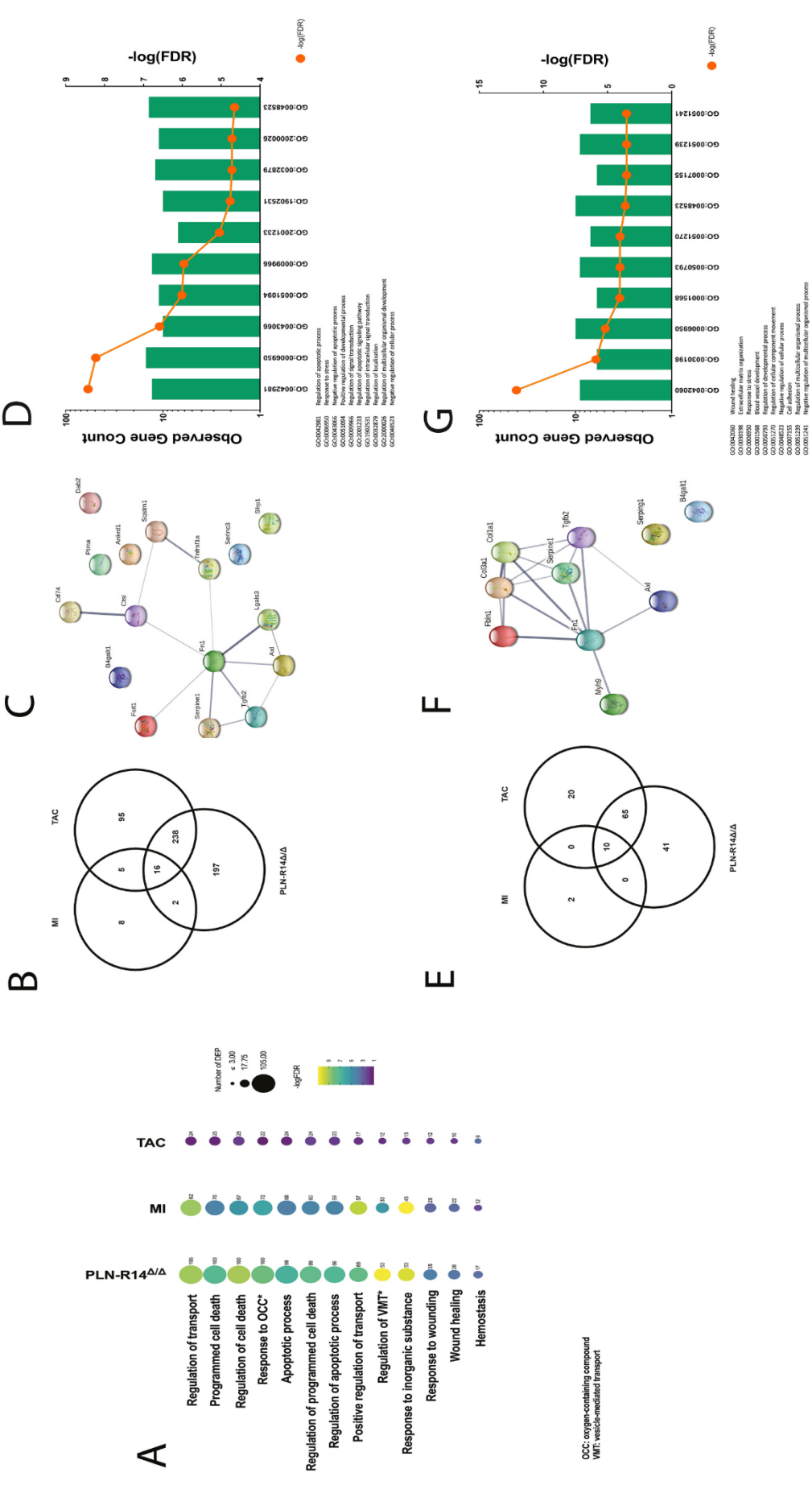

Fig. 5. Bubble plot showing the number of genes and the significance of the shared up-regulated processes in TAC, MI, and PLN-R14$^{\Delta/\Delta}$ (A). The bubble size represents the number of proteins involved in a specific process. Venn diagram representing the number of common up-regulated genes involved in programmed cell death in TAC, MI, and PLN-R14$^{\Delta/\Delta}$ (B). The network analysis between the common up-regulated genes involved in programmed cell death in TAC, MI, and PLN-R14$^{\Delta/\Delta}$ (C). Bar graph representing the number of genes, (from the list of commonly up-regulated genes in programmed cell death in TAC, MI, and PLN-R14$^{\Delta/\Delta}$) observed in specific biological process (only the top 10 processes are shown, based on FDR) (D). Venn diagram representing the number of common up-regulated genes involved in wound healing in TAC, MI, and PLN-R14$^{\Delta/\Delta}$ (E). The network analysis between the common up-regulated genes involved in wound healing in TAC, MI, and PLN-R14$^{\Delta/\Delta}$ (F). Bar graph representing the number of genes, (from the list of commonly up-regulated genes in wound healing in TAC, MI, and PLN-R14$^{\Delta/\Delta}$) observed in specific biological process (only the top 10 processes are shown, based on FDR) (G).

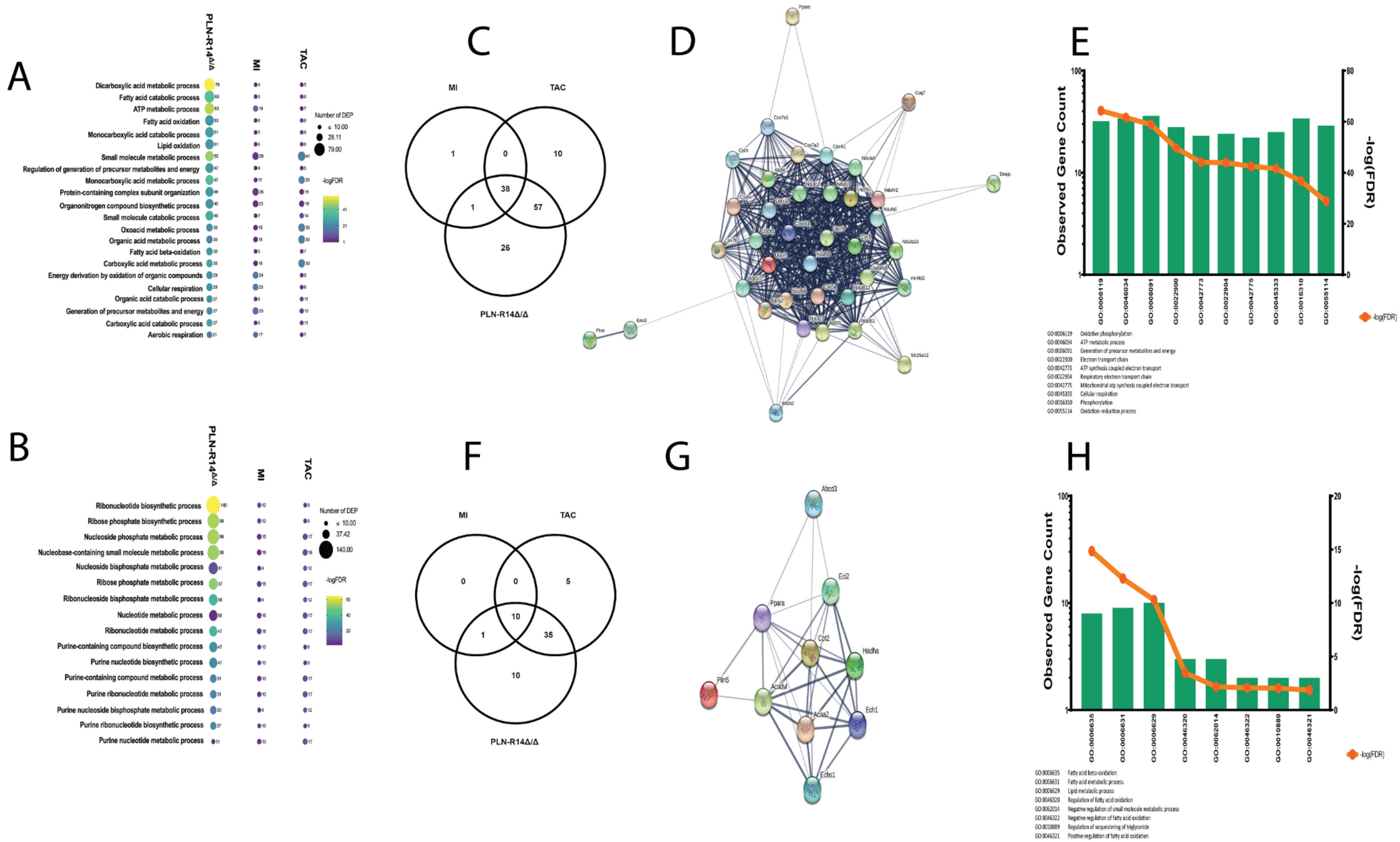

Fig. 6. Bubble plot showing the number of genes and the significance of the shared down-regulated processes in TAC, MI, and PLN-R14$^{\Delta/\Delta}$ (A-B). The bubble size represents the number of proteins involved in a specific process. Venn diagram representing the number of common down-regulated genes involved in ATP metabolic process in TAC, MI, and PLN-R14$^{\Delta/\Delta}$ (C). The network analysis between the common down-regulated genes involved in ATP metabolic process in TAC, MI, and PLN-R14$^{\Delta/\Delta}$ (D). Bar graph representing the number of genes, (from the list of commonly down-regulated genes in ATP metabolic process in TAC, MI, and PLN-R14$^{\Delta/\Delta}$) observed in specific biological process (only the top 10 processes are shown, based on FDR) (E). Venn diagram representing the number of common down-regulated genes involved in lipid oxidation in TAC, MI, and PLN-R14$^{\Delta/\Delta}$ (F). The network analysis between the common down-regulated genes involved in lipid oxidation in TAC, MI, and PLN-R14$^{\Delta/\Delta}$ (G). Bar graph representing the number of genes, (from the list of commonly down-regulated genes in lipid oxidation in TAC, MI, and PLN-R14$^{\Delta/\Delta}$) observed in specific biological process (only the top 10 processes are shown, based on FDR) (H).

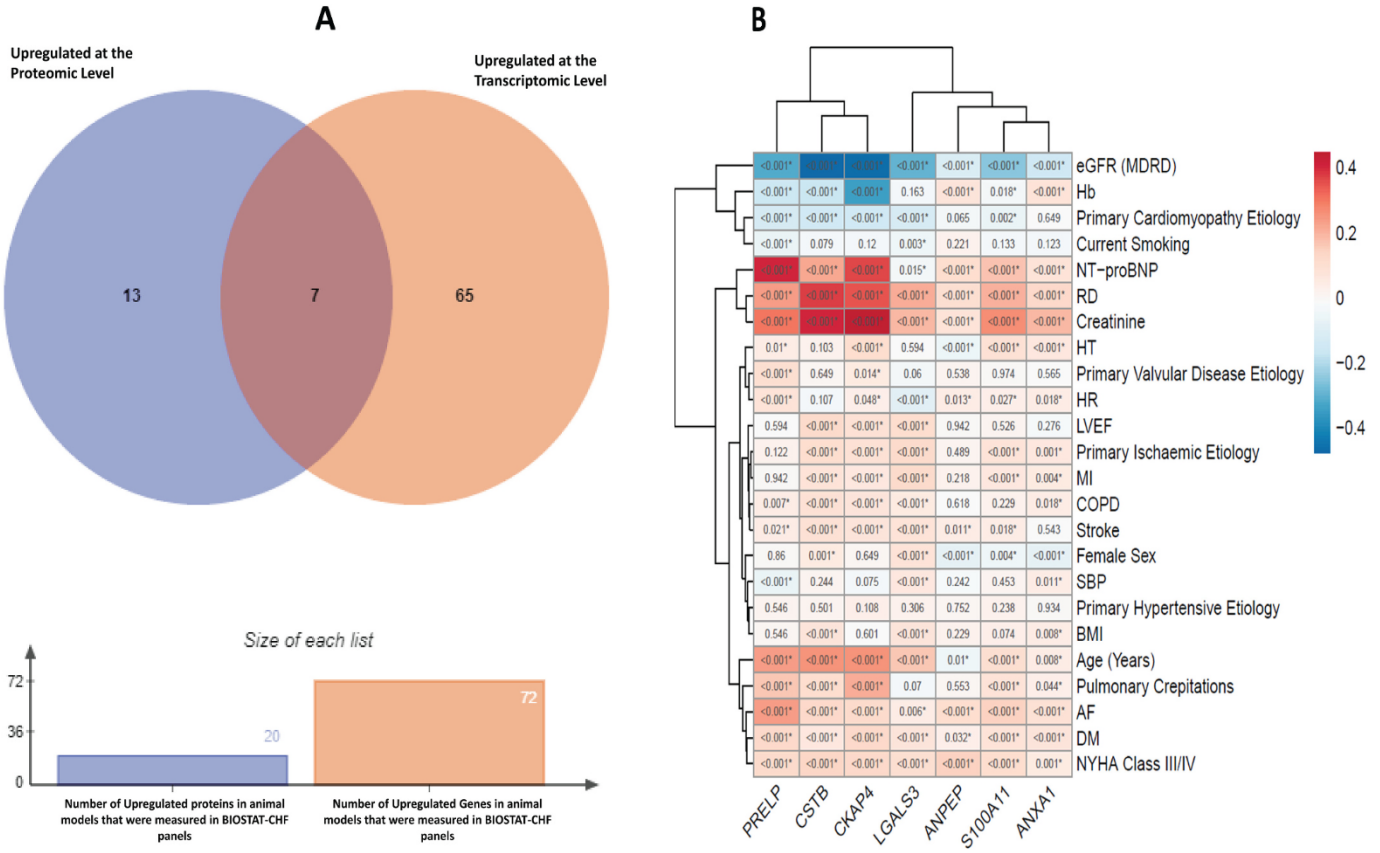

Fig. 7. Venn diagram representing the number of genes that were upregulated at the protein and gene levels in all models and belong to the BIOSTAT-CHF panels (A). Heatmap displaying the correlation of biomarkers with clinical characteristics examined with Spearman's rank order correlation (B). *P*-values of correlation analyses were adjusted for multiple comparisons using the Benjamini-Hochberg method. PRELP: Proline And Arginine Rich End Leucine Rich Repeat Protein; CSTB: Cystatin B; CKAP4: Cytoskeleton Associated Protein 4; LGALS3: Galectin 3; ANPEP: Alanyl Aminopeptidase, Membrane; S100A11: S100 Calcium Binding Protein A11; ANXA1: Annexin A1; eGFR: estimated glomerular filtration rate; NT-proBNP: N-terminal pro-brain natriuretic peptide; Hb: haemoglobin; RD: renal disease; HR: heart rate; LVEF: left ventricular ejection fraction; COPD: chronic obstructive pulmonary disease; SBP: systolic blood pressure; BMI: body mass index; NYHA New York heart association.

Table 4
Results of Cox regression for the combined outcome of all-cause mortality and HF-related rehospitalization, as well as all-cause mortality alone, censored at 2-year follow-up, and competing risks regression for HF-related rehospitalization alone, censored at 2-year follow-up. *p-value ≤0.05.

Biomarkers	Combined Outcome				All-Cause Mortality				HF-Related Rehospitalization			
	Univariable		Multivariable		Univariable		Multivariable		Univariable		Multivariable	
	HR (95% CI)	p-value	HR (95% CI)	p-value	HR (95% CI)	p-value	HR (95% CI)	p-value	HR (95% CI)	p-value	HR (95% CI)	p-value
PRELP	3.76 (3.07, 4.6)	<0.001*	1.72(1.37, 2.16)	<0.001*	4.22(3.26, 5.47)	<0.001*	1.79(1.35, 2.39)	<0.001*	3.51(2.71, 4.55)	<0.001*	1.88(1.4, 2.53)	<0.001*
CSTB	1.41(1.32, 1.49)	<0.001*	1.08(1, 1.16)	0.047*	1.47(1.36, 1.58)	<0.001*	1.08(0.99, 1.19)	0.096	1.41(1.31, 1.52)	<0.001*	1.15(1.05, 1.27)	0.003*
CKAP4	1.69(1.57, 1.83)	<0.001*	1.21(1.09, 1.35)	<0.001*	1.86(1.7, 2.04)	<0.001*	1.38(1.21, 1.57)	<0.001*	1.55(1.35, 1.77)	<0.001*	1.18(1.02, 1.35)	0.023*
LGALS3	1.22(1.11, 1.33)	<0.001*	1.07(0.97, 1.17)	0.156	1.19(1.06, 1.34)	0.003*	1.00(0.89, 1.13)	0.964	1.26(1.13, 1.41)	<0.001*	1.12(0.99, 1.27)	0.063
ANPEP	1.23(1.12, 1.36)	<0.001*	1.03(0.94, 1.14)	0.485	1.25(1.11, 1.41)	<0.001*	1.01(0.89, 1.14)	0.926	1.28(1.13, 1.45)	<0.001*	1.12(0.99, 1.27)	0.083
S100A11	1.56(1.36, 1.79)	<0.001*	1.27(1.09, 1.48)	0.002*	1.67(1.41, 1.97)	<0.001*	1.37(1.13, 1.65)	0.001*	1.47(1.23, 1.75)	<0.001*	1.21(0.99, 1.49)	0.069
ANXA1	1.1(1.01, 1.2)	0.029*	1.04(0.95, 1.15)	0.362	1.2(1.08, 1.33)	<0.001*	1.16(1.04, 1.29)	0.01*	1.04(0.94, 1.16)	0.43	0.98(0.87, 1.11)	0.72

HR hazard ratio; 95% CI 95% confidence interval; PRELP: Proline And Arginine Rich End Leucine Rich Repeat Protein; CSTB: Cystatin B; CKAP4: Cytoskeleton Associated Protein 4; LGALS3: Galectin 3; ANPEP: Alanyl Aminopeptidase, Membrane; S100A11: S100 Calcium Binding Protein A11; ANXA1: Annexin A1.

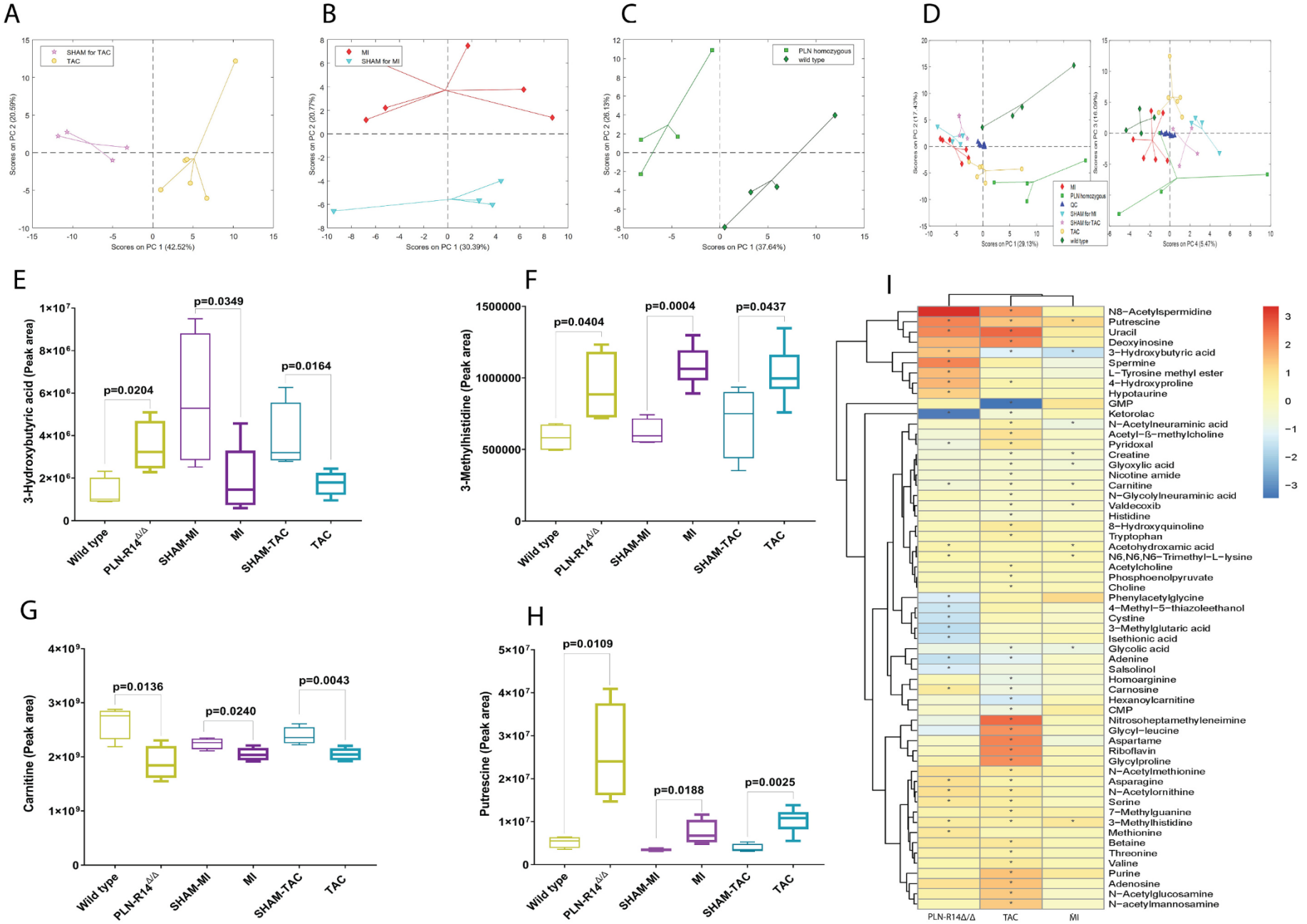

Fig. 8. Differentially expressed metabolites in myocardial tissues. Score plot from PCA model calculated on the relative concentrations of the variables annotated on level 1, 2a or 2b in the reduced dataset For TAC (A), MI (B) and PLN-R14$^{\Delta/\Delta}$ (C) and all models (D). Data has been autoscaled. Box plots representing the differential expression of the metabolites: 3-hydroxybutiric acid (E), 3-Methylhistidine (F) Carnitine (G), and Putrescine (H), and that were significantly ($p < 0.05$) altered in all models.). Data are presented as mean ± SEM. Variables were compared using the *t*-test. A *p*-value <0.05 was considered significant.. Heat map of all metabolites that were altered in each model. Data are presented as logratio of means between a specific model and its corresponding control (I). (TAC: $N = 6$, sham for TAC: $N = 4$; MI: N = 6, sham for MI: N = 4; PLN-R14$^{\Delta/\Delta}$: N = 4, WT: N = 4).

0.0005) (Fig. 8G). 3-hydroxybutyrate (3-OHB) is one of the ketone bodies required to maintain ATP production in the heart [18]. 3-OHB was only upregulated in PLN-R14$^{\Delta/\Delta}$ (2.6-fold higher, $p < 0.05$). However, 3-OHB was downregulated in MI (2.9-fold, $p < 0.05$) and TAC (2.2 -fold, $p < 0.02$) (Fig. 8E).

4. Discussion

We present the first unbiased label-free comparative whole myocardium multi-omics characterization in three different HF mouse models. Omics studies of human myocardial tissues are confounded by several factors, including disease state, tissue genetic heterogeneity [19], comorbidities, and treatments, and are therefore difficult to standardize. One of the main approaches to overcome these problems is using clinically relevant animal models. However, most studies in animal models with unbiased label-free comparative omics presented either transcriptomics, proteomics, or metabolomics, sometimes two, but not all three. Furthermore, most studies reported on one (mouse or rat) model, and this study reports on three common and principal aetiologies of HF: ischemic, pressure overload, and genetic.

The up-regulation of cell death pathways was persistent in all three models at the transcriptomic and proteomic levels. This outcome is in line with previous studies of apoptosis supporting the magnitude of this phenomenon in the progression and worsening of cardiac dysfunction. Narula et al. showed that 5 to 35% of myocytes were affected by apoptosis in patients with ischemic cardiomyopathy and idiopathic dilated cardiomyopathy [20]. Further, Olivetti et al. found that myocardial sections (from the explanted hearts of HF patients undergoing cardiac transplantation) showed a 232-fold increase in myocyte apoptosis and biochemically by DNA laddering [21]. 75% of cardiac cells are non-myocytes, thus, it is essential to establish whether the apoptosis in HF is occurring in myocytes and nonmyocytes. Park et al. revealed in their study that macrophages were the largest fraction of nonmyocytes affected by cell death (41% vs. 18% neutrophils, 16% fibroblast, and 25% endothelial and other cells) [22]. Macroautophagy is a key biological process that modulates stress-induced adaptation and damage control.

The current study revealed that lipids and fatty acid oxidation pathways were downregulated in the myocardial tissues of the three HF mouse models due to both transcriptomic and proteomic changes. As previously discussed [23], HF is characterized by an altered mitochondrial oxidative metabolism. While myocardial fatty acid oxidation is upregulated in HF associated with diabetes and obesity, HF has a reduced fatty acid oxidation in the setting of hypertension or ischemia [24,25].

The altered expression of putrescine and spermine in myocardial tissues confirmed, at the metabolic level, the cell death and cell-repair pathways that were enriched at the transcriptomic and proteomic level (in all three models). Putrescine and spermine are well established for their role in cardiac physiology as key mediators of cell growth, proliferation, and division [15]. Putrescine modulates the acute activation of the beta-adrenergic system in rat hearts [26]. Moreover, carnitine was the only common downregulated metabolite in all three models. Carnitine and its derivatives maintain and protect cardiac metabolism in myocytes by inhibiting the production of free radicals. As discussed elsewhere, carnitine deficiency is a sign of dysfunctional myocardium [27], and carnitine supplementation has been advocated in the past as an adjunct in HF therapy [27,28]. Further, 3-hydroxybutyrate (3-OHB) is one of the ketone bodies required to maintain ATP production in the heart [18]. Its downregulation in surgically-induced HF models could relate to the downregulation of the ATP metabolic process in cardiac tissues.

A modest concordance was detected between transcript and protein levels, especially in TAC mice (53.2% were discordant pairs). This observation could be explained by numerous biological and molecular processes that affect protein levels independently of transcripts, namely translational efficiency, alternative splicing, folding, assembly into complexes, transport, covalent modification, secretion, and degradation [29]. These findings thus emphasise the fact that proteomics and transcriptomics may provide non-overlapping outcomes. Thus, investigators cannot draw robust conclusions based on one type of omic analysis alone, and they should adopt both transcriptomic and proteomic analyses to identify global changes.

Proline And Arginine Rich End Leucine Rich Repeat Protein (PRELP) and Cytoskeleton Associated Protein 4 (CKAP4) showed a strong positive correlation with NT − proBNP levels in HF patients ($p < 0.001$) and predicted all-cause mortality. PRELP, CKAP4, and CSTB were significantly associated with a higher risk of HF-Related Rehospitalization, even after multivariable adjustments. PRELP is normally expressed in the extracellular matrix of collagen-rich tissues like the tendon, lung, and myocardium [30] and interferes with complement pathways. Ahmed et al. reported higher plasma levels of PRELP in HF patients when compared to their controls [31]. Gladka and colleagues supported CKAP4 as a new marker that modulates cardiac fibroblasts during ischemic injury [32]. The prognostic value of cystatin B in HF is poorly understood. One previous study reported an association between CSTB and the risk of coronary events [33].

Our analyses showed an association between Galectin 3 (LGALS3) and all-cause mortality and HF-related rehospitalization. However, this association was not significant after multivariable ajjustment. LGALS3 is a β-galactoside-binding lectin and has been evaluated as a biomarker in heart failure [34,35]. It has been proven that galectin 3 exerts proinflammatory effects and is required for the phagocytic activity of macrophages [36,37]. Besler et al. reported a correlation between myocardial galectin 3 expression and cardiac fibrosis in the left ventricular biopsies of patients with dilated cardiomyopathy [34].

ANXA1 was significantly associated with all-cause mortality and combined outcomes after multivariable adjustment. ANXA1 is an endogenous glucocorticoid-regulated protein that regulates the inflammatory response to restore homeostasis. ANXA1 prevents the infiltration and accumulation of neutrophils by activating neutrophil apoptosis. Also, ANXA1 stimulates monocyte recruitment and apoptotic leukocyte clearance by macrophages [38]. The pre-clinical study of Ferraro et al. advocated the beneficial role of ANXA1 in establishing a reparative phenotype, inducing angiogenesis, and hampering the accumulation of inflammatory macrophages after MI [39]. To conclude, ANXA1 exhibits central role in the modulation of apoptosis and injury repair in HF. This outcome supports the trends of the cell-death and tissue-repair pathways that were enriched in the myocardial tissues of PLN-R14$^{\Delta/\Delta}$, MI, and TAC.

5. Study limitations

The approach followed in this study, although extensive, has a number of limitations. In this study, all three HF mouse models were male mice and represented one time point (tissues were harvested six weeks after surgery). Replicating all experiments in female mice and checking changes at differen timepoints mice would make the analysis and the inclusion of all data very challenging. Therefore, we encourage future studies to assess the sex differences in each of model and check for molecular changes at different timepoints. Moreover, data produced by omics methods lead to inevitable difficulties in data interpretation. In this regard, bias and selective reporting need to be stressed as general limitations of large datasets. Thus, confirmation of findings from omics studies in future scientific research, particularly focusing on a selection of identified genes/proteins of interest, is necessary to definitively establish their significance. On a related note, while the applied pathway analysis tools can assist with disentangling the inherent complexity of omics data, these are also subject to limitations of their own, such as the definition of cut-off points for determining biological significance.

Another issue is that databases used for pathway analyses are based

on annotations from available scientific publications, which might lead to over-representation of certain annotations that have been studied more extensively. In addition, since annotations are based on published literature, they are also subject to the limitations of said literature. Lastly, network-based approaches for multi-omics data analyses is another challenge of multi-omics integration [40].

With regard to the clinical data used in this study, a potential limitation is that the not all of the identified hits at the RNA or protein level could be investigated in humans, as the Olink panels contain only a selection of specific biomarkers and not the entire human proteome. As such, the potential clinical and prognostic associations of some of the findings of our study will need to be independently investigated in the future.

In this study, the two surgery-induced models were performed on mice with the same age and strain, as well as at the same time points. For the "homozygous" PLN-R14$^{\Delta/\Delta}$ model, the mice develop a severe phenotype at the age of 7 weeks and die shortly afterward and as such, we cannot apply the same timepoints in their case [5]. In addition, the sham procedure for the TAC model is different from the sham procedure for the MI model. Thus, taking these points into account, we deduced that the most appropriate approach to determine the regulated genes would be to compare each model to its corresponding control group. By using this approach, we can essentially eliminate model- or surgery-specific artefacts. For the transcriptomic data, all possible pairwise comparisons between control groups are made available in the supplementary file.

Finally,mass spectrometry-based proteomic analyses and antibody-based methods are fundamentally different methods. Thus, the validation of Mass spectrometry-based proteomics by antibody-based methods is not effective and often leads to discrepancies. The Mass spectrometry-based proteomic method, adopted in this study, demonstrates many advantages over the conventionally used antibody-based methods, like enzyme-linked immunosorbent assay (ELISA) and Western blot (WB), and they deliver greater specificity and reproducibility [41]. Moreover, ELISA and WB rely on the availability of specific antibodies, which are poor, not existent for many proteins, or limited by the number of antigens/specific epitopes they can probe [42]. Therefore, the validation should be confined to reproduction with the same method in other animal models and in human samples.

6. Conclusions

In a multi-omics analysis of heart tissues from 3 distinct animal models of HF, biological processes related to cell death and wound healing were significantly upregulated, and metabolic processes were significantly downregulated in all models. However, varying amounts of discordance between the RNA (transcriptomics) and protein (proteomics) levels were identified, with more than half of RNA/protein pairs being discordant in the TAC model (RNA upregulated and protein downregulated or the opposite). This finding emphasises the need to confirm findings from the RNA level at the protein level and vice-versa. To conlude, the pharmacological targeting of the identified common pathways, maily cell death and metabolic processes represents a promising therapeutic approach to improve cardiac efficiency and function in heart failure. Also, the differentially expressed biomarkers with potential clinical and prognostic associations merit further exploration to understand their role in the pathophysiology of HF.

Funding

This work was by a grant from the European Research Council (ERC CoG 818715, SECRETE-HF). Furthermore, supported by grants from the Netherlands Heart Foundation (CVON SHE-PREDICTS-HF, grant 2017–21; CVON RED-CVD, grant 2017–11; CVON PREDICT2, grant 2018–30; and CVON DOUBLE DOSE, grant 2020B005), by a grant from the leDucq Foundation (Cure PhosphoLambaN induced Cardiomyopathy (Cure-PLaN). Canxia Shi is supported by a scholarship from the China Scholarship Council (CSC number: 201806170057).

Declaration of Competing Interest

The UMCG, which employs several of the authors, has received research grants and/or fees from AstraZeneca, Abbott, Boehringer Ingelheim, Cardior Pharmaceuticals Gmbh, Ionis Pharmaceuticals, Inc., Novo Nordisk, and Roche. Dr. de Boer received speaker fees from Abbott, AstraZeneca, Bayer, Novartis, and Roche.

Appendix A. Supplementary data

Supplementary data to this article can be found online at https://doi.org/10.1016/j.yjmcc.2022.12.001.

References

[1] J.E. Ho, D. Enserro, F.P. Brouwers, J.R. Kizer, S.J. Shah, B.M. Psaty, T.M. Bartz, R. Santhanakrishnan, D.S. Lee, C. Chan, K. Liu, M.J. Blaha, H.L. Hillege, P. van der Harst, W.H. van Gilst, W.J. Kop, R.T. Gansevoort, R.S. Vasan, J.M. Gardin, D. Levy, J.S. Gottdiener, R.A. de Boer, M.G. Larson, Predicting heart failure with preserved and reduced ejection fraction: the international collaboration on heart failure subtypes, Circ. Heart Fail. 9 (6) (2016).

[2] G. Lippi, F. Sanchis-Gomar, Global epidemiology and future trends of heart failure, AME Med. J. 5 (2020) 15.

[3] E. Vanoli, S. Bacchini, S. Panigada, F. Pentimalli, P. Adamson, Experimental models of heart failure, Eur. Heart J. Suppl. 6 (2004) F7–F15.

[4] C. Riehle, J. Bauersachs, Small animal models of heart failure, Cardiovasc. Res. 115 (13) (2019) 1838–1849.

[5] T.R. Eijgenraam, B.J. Boukens, C.J. Boogerd, E.M. Schouten, C.W.A. van de Kolk, N.M. Stege, W.P. Te Rijdt, E.T. Hoorntje, P.A. van der Zwaag, E. van Rooij, J.P. van Tintelen, M.P. van den Berg, P. van der Meer, J. van der Velden, H.H.W. Sillje, R. A. de Boer, The phospholamban p.(Arg14del) pathogenic variant leads to cardiomyopathy with heart failure and is unreponsive to standard heart failure therapy, Sci. Rep. 10 (1) (2020) 9819.

[6] G. Markousis-Mavrogenis, J. Tromp, W. Ouwerkerk, M. Devalaraja, S.D. Anker, J. G. Cleland, K. Dickstein, G.S. Filippatos, P. van der Harst, C.C. Lang, M. Metra, L. L. Ng, P. Ponikowski, N.J. Samani, F. Zannad, A.H. Zwinderman, H.L. Hillege, D. J. van Veldhuisen, R. Kakkar, A.A. Voors, P. van der Meer, The clinical significance of interleukin-6 in heart failure: results from the BIOSTAT-CHF study, Eur. J. Heart Fail. 21 (8) (2019) 965–973.

[7] A.A. Voors, S.D. Anker, J.G. Cleland, K. Dickstein, G. Filippatos, P. van der Harst, H.L. Hillege, C.C. Lang, J.M. Ter Maaten, L. Ng, P. Ponikowski, N.J. Samani, D. J. van Veldhuisen, F. Zannad, A.H. Zwinderman, M. Metra, A systems BIOlogy study to TAilored treatment in chronic heart failure: rationale, design, and baseline characteristics of BIOSTAT-CHF, Eur. J. Heart Fail. 18 (6) (2016) 716–726.

[8] G. Markousis-Mavrogenis, J. Tromp, W. Ouwerkerk, J.P. Fereirra, S.D. Anker, J. G. Cleland, K. Dickstein, G. Filippatos, C.C. Lang, M. Metra, N.J. Samani, B.-C. Consortium, R.A. De Boer, D.J. Van Veldhuisen, A.A. Voors, P. Van Der Meer, Multimarker profiling identifies protective and harmful immune processes in heart failure: findings from BIOSTAT-CHF, Cardiovasc. Res. 118 (8) (2021) 1964–1977. https. //www.ncbi.nlm.nih.gov/pmc/articles/PMC9239579/.

[9] A.A. Voors, W. Ouwerkerk, F. Zannad, D.J. van Veldhuisen, N.J. Samani, P. Ponikowski, L.L. Ng, M. Metra, J.M. Ter Maaten, C.C. Lang, H.L. Hillege, P. van der Harst, G. Filippatos, K. Dickstein, J.G. Cleland, S.D. Anker, A.H. Zwinderman, Development and validation of multivariable models to predict mortality and hospitalization in patients with heart failure, Eur. J. Heart Fail. 19 (5) (2017) 627–634.

[10] C. Kilkenny, W.J. Browne, I.C. Cuthill, M. Emerson, D.G. Altman, Improving bioscience research reporting: the ARRIVE guidelines for reporting animal research, PLoS Biol. 8 (6) (2010), e1000412.

[11] A. van der Pol, A. Gil, H.H.W. Sillje, J. Tromp, E.S. Ovchinnikova, I. Vreeswijk-Baudoin, M. Hoes, I.J. Domian, B. van de Sluis, J.M. van Deursen, A.A. Voors, D. J. van Veldhuisen, W.H. van Gilst, E. Berezikov, P. van der Harst, R.A. de Boer, R. Bischoff, P. van der Meer, Accumulation of 5-oxoproline in myocardial dysfunction and the protective effects of OPLAH, Sci. Transl. Med. 9 (415) (2017).

[12] W. Du, A. Piek, E.M. Schouten, C.W.A. van de Kolk, C. Mueller, A. Mebazaa, A. A. Voors, R.A. de Boer, H.H.W. Sillje, Plasma levels of heart failure biomarkers are primarily a reflection of extracardiac production, Theranostics 8 (15) (2018) 4155–4169.

[13] S.X. Ge, D. Jung, R. Yao, ShinyGO: a graphical gene-set enrichment tool for animals and plants, Bioinformatics 36 (8) (2020) 2628–2629.

[14] T.R. Eijgenraam, C.J. Boogerd, N.M. Stege, V. Oliveira Nunes Teixeira, M. M. Dokter, L.E. Schmidt, X. Yin, K. Theofilatos, M. Mayr, P. van der Meer, E. van Rooij, J. van der Velden, H.H.W. Sillje, R.A. de Boer, Protein Aggregation Is an Early Manifestation of Phospholamban p.(Arg14del)-Related Cardiomyopathy: Development of PLN-R14del-Related Cardiomyopathy, Circ. Heart Fail. 14 (11) (2021), https://doi.org/10.1161/CIRCHEARTFAILURE.121.008532 e008532.

[15] C. Meana, J.M. Rubin, C. Bordallo, L. Suarez, J. Bordallo, M. Sanchez, Correlation between endogenous polyamines in human cardiac tissues and clinical parameters in patients with heart failure, J. Cell. Mol. Med. 20 (2) (2016) 302–312.
[16] D.J. Paulson, Carnitine deficiency-induced cardiomyopathy, Mol. Cell. Biochem. 180 (1–2) (1998) 33–41.
[17] M.A. Martin, M.A. Gomez, F. Guillen, B. Bornstein, Y. Campos, J.C. Rubio, C.S. de la Calzada, J. Arenas, Myocardial carnitine and carnitine palmitoyltransferase deficiencies in patients with severe heart failure, Biochim. Biophys. Acta 1502 (3) (2000) 330–336.
[18] R. Nielsen, N. Moller, L.C. Gormsen, L.P. Tolbod, N.H. Hansson, J. Sorensen, H. J. Harms, J. Frokiaer, H. Eiskjaer, N.R. Jespersen, S. Mellemkjaer, T.R. Lassen, K. Pryds, H.E. Botker, H. Wiggers, Cardiovascular effects of treatment with the ketone body 3-Hydroxybutyrate in chronic heart failure patients, Circulation 139 (18) (2019) 2129–2141.
[19] J. Hesse, C. Owenier, T. Lautwein, R. Zalfen, J.F. Weber, Z. Ding, C. Alter, A. Lang, M. Grandoch, N. Gerdes, J.W. Fischer, G.W. Klau, C. Dieterich, K. Kohrer, J. Schrader, Single-cell transcriptomics defines heterogeneity of epicardial cells and fibroblasts within the infarcted murine heart, Elife 10 (2021).
[20] J. Narula, N. Haider, R. Virmani, T.G. DiSalvo, F.D. Kolodgie, R.J. Hajjar, U. Schmidt, M.J. Semigran, G.W. Dec, B.A. Khaw, Apoptosis in myocytes in end-stage heart failure, N. Engl. J. Med. 335 (16) (1996) 1182–1189.
[21] M. Richter, S. Kostin, The failing human heart is characterized by decreased numbers of telocytes as result of apoptosis and altered extracellular matrix composition, J. Cell. Mol. Med. 19 (11) (2015) 2597–2606.
[22] M. Park, Y.T. Shen, V. Gaussin, G.R. Heyndrickx, J. Bartunek, R.R. Resuello, F. F. Natividad, R.N. Kitsis, D.E. Vatner, S.F. Vatner, Apoptosis predominates in nonmyocytes in heart failure, Am. J. Physiol. Heart Circ. Physiol. 297 (2) (2009) H785–H791.
[23] G.D. Lopaschuk, Q.G. Karwi, R. Tian, A.R. Wende, E.D. Abel, Cardiac energy metabolism in heart failure, Circ. Res. 128 (10) (2021) 1487–1513.
[24] H. Tuunanen, E. Engblom, A. Naum, K. Nagren, B. Hesse, K.E. Airaksinen, P. Nuutila, P. Iozzo, H. Ukkonen, L.H. Opie, J. Knuuti, Free fatty acid depletion acutely decreases cardiac work and efficiency in cardiomyopathic heart failure, Circulation 114 (20) (2006) 2130–2137.
[25] H. Wiggers, M. Halbirk, H. Norrelund, Letter by Wiggers et al regarding article by Tuunanen et al, "free fatty acid depletion acutely decreases cardiac work and efficiency in cardiomyopathic heart failure", Circulation 115 (21) (2007) (e545; author reply e547).
[26] C. Bordallo, B. Cantabrana, L. Velasco, L. Secades, C. Meana, M. Mendez, J. Bordallo, M. Sanchez, Putrescine modulation of acute activation of the beta-adrenergic system in the left atrium of rat, Eur. J. Pharmacol. 598 (1–3) (2008) 68–74.
[27] R. Lango, R.T. Smolenski, M. Narkiewicz, J. Suchorzewska, W. Lysiak-Szydlowska, Influence of L-carnitine and its derivatives on myocardial metabolism and function in ischemic heart disease and during cardiopulmonary bypass, Cardiovasc. Res. 51 (1) (2001) 21–29.
[28] X. Song, H. Qu, Z. Yang, J. Rong, W. Cai, H. Zhou, Efficacy and safety of L-carnitine treatment for chronic heart failure: a Meta-analysis of randomized controlled trials, Biomed. Res. Int. 2017 (2017) 6274854.
[29] A. Ghazalpour, B. Bennett, V.A. Petyuk, L. Orozco, R. Hagopian, I.N. Mungrue, C. R. Farber, J. Sinsheimer, H.M. Kang, N. Furlotte, C.C. Park, P.Z. Wen, H. Brewer, K. Weitz, D.G. Camp 2nd, C. Pan, R. Yordanova, I. Neuhaus, C. Tilford, N. Siemers, P. Gargalovic, E. Eskin, T. Kirchgessner, D.J. Smith, R.D. Smith, A.J. Lusis, Comparative analysis of proteome and transcriptome variation in mouse, PLoS Genet. 7 (6) (2011), e1001393.
[30] A. Hultgardh-Nilsson, J. Boren, S. Chakravarti, The small leucine-rich repeat proteoglycans in tissue repair and atherosclerosis, J. Intern. Med. 278 (5) (2015) 447–461.
[31] A. Ahmed, S. Ahmed, M. Arvidsson, H. Bouzina, J. Lundgren, G. Radegran, Prolargin and matrix metalloproteinase-2 in heart failure after heart transplantation and their association with haemodynamics, ESC Heart Fail 7 (1) (2020) 223–234.
[32] M.M. Gladka, B. Molenaar, H. de Ruiter, S. van der Elst, H. Tsui, D. Versteeg, G.P. A. Lacraz, M.M.H. Huibers, A. van Oudenaarden, E. van Rooij, Single-cell sequencing of the healthy and diseased heart reveals cytoskeleton-associated protein 4 as a new modulator of fibroblasts activation, Circulation 138 (2) (2018) 166–180.
[33] I. Goncalves, K. Hultman, P. Duner, A. Edsfeldt, B. Hedblad, G.N. Fredrikson, H. Bjorkbacka, J. Nilsson, E. Bengtsson, High levels of cathepsin D and cystatin B are associated with increased risk of coronary events, Open Heart 3 (1) (2016), e000353.
[34] Rudolf A. de Boer, Adriaan A. Voors, Pieter Muntendam, Wiek H. van Gilst, Dirk J. van Veldhuisen, Galectin-3: a novel mediator of heart failure development and progressio, European Journal of Heart Failure 11 (9) (2009) 811–817, https://doi.org/10.1093/eurjhf/hfp097.
[35] R.A. de Boer, D.J. Lok, T. Jaarsma, P. van der Meer, A.A. Voors, H.L. Hillege, D. J. van Veldhuisen, Predictive value of plasma galectin-3 levels in heart failure with reduced and preserved ejection fraction, Ann. Med. 43 (1) (2011) 60–68.
[36] U.C. Sharma, S. Pokharel, T.J. van Brakel, J.H. van Berlo, J.P. Cleutjens, B. Schroen, S. Andre, H.J. Crijns, H.J. Gabius, J. Maessen, Y.M. Pinto, Galectin-3 marks activated macrophages in failure-prone hypertrophied hearts and contributes to cardiac dysfunction, Circulation 110 (19) (2004) 3121–3128.
[37] K. Reifenberg, H.A. Lehr, M. Torzewski, G. Steige, E. Wiese, I. Kupper, C. Becker, S. Ott, P. Nusser, K. Yamamura, G. Rechtsteiner, T. Warger, A. Pautz, H. Kleinert, A. Schmidt, B. Pieske, P. Wenzel, T. Munzel, J. Lohler, Interferon-gamma induces chronic active myocarditis and cardiomyopathy in transgenic mice, Am. J. Pathol. 171 (2) (2007) 463–472.
[38] M.A. Sugimoto, J.P. Vago, M.M. Teixeira, L.P. Sousa, Annexin A1 and the resolution of inflammation: modulation of neutrophil recruitment, apoptosis, and clearance, J Immunol Res 2016 (2016) 8239258.
[39] B. Ferraro, G. Leoni, R. Hinkel, S. Ormanns, N. Paulin, A. Ortega-Gomez, J.R. Viola, R. de Jong, D. Bongiovanni, T. Bozoglu, S.L. Maas, M. D'Amico, T. Kessler, T. Zeller, M. Hristov, C. Reutelingsperger, H.B. Sager, Y. Doring, M. Nahrendorf, C. Kupatt, O. Soehnlein, Pro-Angiogenic macrophage phenotype to promote myocardial repair, J. Am. Coll. Cardiol. 73 (23) (2019) 2990–3002.
[40] F.R. Pinu, D.J. Beale, A.M. Paten, K. Kouremenos, S. Swarup, H.J. Schirra, D. Wishart, Systems Biology and multi-omics integration: viewpoints from the metabolomics research community, Metabolites 9 (4) (2019).
[41] T. Jayasena, A. Poljak, N. Braidy, L. Zhong, B. Rowlands, J. Muenchhoff, R. Grant, G. Smythe, C. Teo, M. Raftery, P. Sachdev, Application of targeted mass spectrometry for the quantification of Sirtuins in the central nervous system, Sci. Rep. 6 (2016) 35391.
[42] W. Timp, G. Timp, Beyond mass spectrometry, the next step in proteomics, Sci. Adv. 6 (2) (2020) eaax8978.